ORIGINAL ARTICLE

WILEY Plant, Cell & Environment PCE

A network model links wood anatomy to xylem tissue hydraulic behaviour and vulnerability to cavitation

Assaad Mrad[1] | Jean-Christophe Domec[1,2] | Cheng-Wei Huang[3] | Frederic Lens[4] |
Gabriel Katul[1]

[1] Nicholas School of the Environment, Duke University, Durham, NC 27708, USA

[2] Bordeaux Sciences Agro, UMR 1391 INRA-ISPA, 33175 Gradignan Cedex, France

[3] Department of Biology, University of New Mexico, Albuquerque, NM 87131-0001

[4] Naturalis Biodiversity Center, Leiden University, P.O. Box 9517, 2300 RA Leiden, The Netherlands

Correspondence
Assaad Mrad, Nicholas School of the Environment, Duke University, Durham, NC 27708, USA.
Email: mradassaad2@gmail.com

Abstract

Plant xylem response to drought is routinely represented by a vulnerability curve (VC). Despite the significance of VCs, the connection between anatomy and tissue-level hydraulic response to drought remains a subject of inquiry. We present a numerical model of water flow in flowering plant xylem that combines current knowledge on diffuse-porous anatomy and embolism spread to explore this connection. The model produces xylem networks and uses different parameterizations of intervessel connection vulnerability to embolism spread: the Young–Laplace equation and pit membrane stretching. Its purpose is upscaling processes occurring on the microscopic length scales, such as embolism propagation through pit membranes, to obtain tissue-scale hydraulics. The terminal branch VC of *Acer glabrum* was successfully reproduced relying only on real observations of xylem tissue anatomy. A sensitivity analysis shows that hydraulic performance and VC shape and location along the water tension axis are heavily dependent on anatomy. The main result is that the linkage between pit-scale and vessel-scale anatomical characters, along with xylem network topology, affects VCs significantly. This work underscores the importance of stepping up research related to the three-dimensional network structure of xylem tissues. The proposed model's versatility makes it an important tool to explore similar future questions.

KEYWORDS

xylem, network, *Acer*, model, hydraulics, cavitation, vulnerability curve, wood, anatomy

1 | INTRODUCTION

"Vessels and tracheids normally contain both air and water, the relative amounts of the two substances varying according to the season and the time of day." Since Haberlandt wrote this statement in 1914 (Haberlandt & Drummond, 1914), we have slowly come to understand that cavitation events, or the formation of emboli, play a major part in plant survival and distribution (Adams et al., 2017; Anderegg et al., 2016; Choat et al., 2012). However, despite decades of research, describing water movement within plant tissues remains a formidable scientific challenge given the high degree of complexity of the xylem system, which evolved under complex physical, chemical, and biological pressures (Lucas et al., 2013). Xylem tissues are

specialized to transport water efficiently by offering the least possible resistance to flow yet not allowing water potential to drop below thresholds required for hydraulic safety. This goal is met by different transport designs with ancestral vascular plants evolving towards extant gymnosperms and angiosperms, including unicellular (tracheids) and multicellular structures (vessels), connected through porous intervessel pits of varying complexity (Choat, Cobb, & Jansen, 2008; Sperry, 2003).

However, sufficient water transport is not guaranteed when evaporative demand by the atmosphere exceeds root water supply to the leaf over long periods (Manzoni, Katul, & Porporato, 2014). The persistent long-term imbalance between atmospheric demand and supply of water from the soil reservoir triggers embolism or

unstable bubble formation in the conducting xylem tissues due to increases in xylem water tension (Meinzer, Clearwater, & Goldstein, 2001). Depending on the species, the tension sustained by the ascending sap in the xylem of trees can reach more than 20 MPa during periods of water stress (Larter et al., 2015). Under these conditions, water is in a metastable state and cavitation can occur, leading to embolism. Embolism occurs when the aforementioned water tension in the xylem increases enough to allow air entry into vessels (Tyree & Zimmermann, 2002). If a plant is unable to prevent the spread of embolism over extended periods, this may be a tipping point towards drought-induced mortality.

The vulnerability of a plant organ (often root, stem, or branch) to water stress is represented by a so-called vulnerability to cavitation curve (Tyree & Zimmermann, 2002; Sperry, 2011), a plot that features loss in relative conductivity with increasing liquid tension and represents an integration of emboli over hundreds to thousands of xylem vessels. The shape of vulnerability curves (VCs) and its possible connection to wood anatomical traits is currently a subject of active research given the rapid development of measuring techniques for VCs and the capacity to image wood traits and embolism formation at unprecedented resolution (Brodersen & Roddy, 2016; Cai, Li, Zhang, Zhang, & Tyree, 2014; Knipfer, Brodersen, Zedan, Kluepfel, & McElrone, 2015; McElrone, Choat, Parkinson, MacDowell, & Brodersen, 2013). Plant hydraulic traits, in general, and xylem resistance to cavitation, in particular, have been shown to be diverse across many plant taxa experiencing drought induced mortality (Adams et al., 2017; Johnson et al., 2018).

The vessels in the xylem of flowering plants form a network through which water travels from roots to leaves. Although every individual plant has its own xylem network topology (relative position of vessels to each other), individuals of the same species with comparable age and habitat possess similar anatomical statistics such as average vessel length and diameter at a given position in the same plant organ (Hunt & Manzoni, 2015). In a typical flowering plant, there exist anatomical elements on two widely separated length scales that simultaneously affect whole plant hydraulic conductivity and vulnerability to embolism. The first are the vessel-scale size distributions comprising the vessel lengths and diameters whose averages are of the order of 10 cm and 10 μm, respectively, in the case of the genus *Acer* (Jacobsen, Pratt, Tobin, Hacke, & Ewers, 2012; Lens et al., 2011). The second are the pit-scale size distributions including the diameter of intervessel pit membrane pores spanning 1 nm to more than 100 nm and those of the pit membranes containing them three order of magnitudes larger (Hacke, Sperry, Wheeler, & Castro, 2006; Sperry & Hacke, 2004). Even though pits and vessel sizes differ by one to eight orders of magnitude (from a 1-nm-wide intervessel pit pore to a 10-cm-long vessel), the extent of their effect on plant hydraulics and VCs are both substantial. The interaction among them in a network gives rise to stem-scale hydraulic properties such as conductivity and vulnerability to drought (ergo VCs). Because hydraulic failure is impacted by this wide range of scales, upscaling from wood anatomy to branch and plant level requires novel theoretical and modelling tactics. One controversial link between the two ranges of length scales is the rare-pit hypothesis. This hypothesis stipulates that species with large mean

intervessel pit areas are more likely to possess large pores in their contact wall allowing easier bubble propagation which in turn makes these species more vulnerable to cavitation than ones with smaller mean pit areas. Since the introduction of an equivalent concept, the pit area hypothesis, in an article focusing on the species of the family *Rosaceae* (Wheeler, Sperry, Hacke, & Hoang, 2005), a subsequent study that includes several other genera in and outside *Rosaceae* found a decreasing statistical significance for the correlation between mean intervessel pit area and metrics of plant vulnerability to cavitation (Scholz et al., 2013). However, it is still plausible to assume that within a plant tissue, vessels with large pit area A_p are more vulnerable than their smaller counterparts within that same tissue (Christman, Sperry, & Adler, 2009). In contrast to previous studies, here, A_p refers to a single vessel's pit area as opposed to the mean pit area of the whole xylem tissue. This conjecture is not a juxtaposition of interspecies or intraspecies vulnerability to cavitation but merely describes the stochastic component of cavitation resistance at the vessel level within the same plant tissue.

The goal here is to explore connections between wood anatomical characters and segment scale hydraulics using an efficient newly developed numerical model that explicitly takes vessel connectivity and network topology into account. The main advantage of this model is that it uses only real anatomical measurements, such as vessel length and diameter distributions, of a flowering plant to produce results. The model does not rely on macroscopic data such as whole-segment hydraulic conductivity and VCs. The knowledge gained here provides a novel perspective that addresses many aspects of resistance to embolism. In particular, this work answers the following questions: (a) How does the model upscale hydraulic properties with two perspectives of cavitation resistance at the pit membrane level? (b) What is the effect of the linkage between vessel-level and pit-level anatomy on the shape of the VC?

The model is first fed with anatomical observations of *Acer glabrum* to create a random xylem network on a two-dimensional grid. Then, a series of simulations are run on the generated network to extract its hydraulic properties. A sensitivity analysis of the model shows the connection between pit- and vessel-scale properties and drought-induced loss of conductivity (or the VC shape) on the tissue-scale. The model allows turning "on" or "off" the effects of various mechanisms at the appropriate scale thereby discerning on their role in shaping VCs. As such, rigorous microscopic laws, such as embolism propagation, are integrated along the water pathway to predict the macroscopic form of VCs (Katul, Porporato, & Oren, 2007).

2 | DESCRIPTION

A model of diffuse-porous xylem was developed and available at: https://github.com/mradassaad/Xylem_Network_Matlab. The model is a two-dimensional representation of a network with features capturing much of the current knowledge on xylem anatomy. It has two functions: (a) to generate a random xylem network using empirical anatomical statistics (Table 1) and (b) to measure hydraulic properties and vessel water relations. The network generation approach is based

TABLE 1 Nomenclature and description of the model parameters

Name	Description	Value	Unit
Vessels			
D_v	Average vessel diameter	24.6	µm
$D_{v,cv}$	Coefficient of variation of vessel diameters	0.12	dimensionless
P_v	Probability of ending a vessel	0.86	dimensionless
NP_v	Probability of starting a vessel	0.83	dimensionless
intervessel connections (IVCs)			
D_p	Average pore size	32	nm
D_m	Average pit membrane diameter	6.3	µm
f_c	Fraction of vessel area in contact with other vessels	0.31	dimensionless
f_{pf}	Fraction of contact area occupied by pits	0.7	dimensionless
f_{ap}	Ratio of aperture area to pit membrane area	0.06	dimensionless
T_m	Pit membrane thickness	234	nm
L_p	Pit chamber depth	635	nm
L_{ve}	Length of a vessel element	2	mm
a	Weibull parameter in Equation (7)	20.28	MPa
b	Weibull parameter in Equation (7)	3.2	dimensionless
P_e	Probability of building an IVC	0.4	dimensionless
e_{mean}	Mean membrane strain required for air-seeding	0.015	dimensionless
e_{cv}	Coefficient of variation of membrane strains required for air-seeding	0.35	dimensionless
Dimension of simulated segment			
Rows	Number of grid rows	100	dimensionless
Columns	Number of grid columns	1,000	dimensionless
General constants			
γ	Surface tension of water-air interface at 20°C	0.072	Pa.m
μ	Viscosity of water at 20°C	0.001	Pa.s
E	Modulus of elasticity of pit membrane	400	MPa
υ	Poisson ratio	0.3	dimensionless

Note. Values shown are either from the measured anatomy of *Acer glabrum* reported in Lens et al., 2011 or tuned to obtain satisfactory xylem network properties (in bold) except for E and υ taken from Tixier et al., 2014.

on the model in Loepfe, Martinez-Vilalta, Piñol, & Mencuccini (2007) with modifications introduced to elucidate how anatomy and different parameterizations of pit membrane cavitation resistance affect VC location along the pressure axis and shape or curvature.

2.1 | Xylem network structure

Figure 1a illustrates how vessels provide a one-directional pathway for water as it flows from roots to leaves. There exist common or shared walls between different vessels called contact walls. Contact walls between two vessels (Figure 1a, in green) are subdivided into several intervessel pit areas (A_p; Figure 1a, in red). Pit areas consist of pit membranes of specified diameter D_m including pores of different sizes (Figure 1c). We denote the average of the pore diameters as D_p and their maximum as $D_{p, max}$. The pit membranes and their pores have two hydraulic functions: (a) They provide a pathway for water to move from vessel to vessel and (b) they protect vessels from embolism spread (Choat, Brodie, Cobb, Zwieniecki, & Holbrook, 2006; Hacke et al., 2006; Sperry & Hacke, 2004; Tyree & Zimmermann, 2002; Wheeler et al., 2005). When water reaches a contact wall, it passes through the pores to the adjacent vessel (after encountering energy losses) and can continue its ascent towards the leaves.

Figure 1b shows a close-up on one of the many possible model-generated networks and its corresponding terms in relation to their equivalents in plant anatomy. The bottom end of the network is considered the inlet and the upper end the outlet. There are two primary elements involved in this modelling approach: vessels (in black) and intervessel connections (IVCs; in red). Clusters are defined as a collection of vessels and IVCs that independently carry water from inlet to outlet. It is possible for more than one IVC to link the same two vessels. The collection of these IVCs forms a contact wall between the two vessels. For example, if three vertically consecutive IVCs connect the same two vessels then that contact area spans these three vessel elements. Therefore, IVCs are portions of contact walls.

2.2 | Xylem network generation

The proposed modelling approach generates a network of vessels connected by IVCs, mimicking diffuse-porous angiosperm xylem architecture on a grid of nodes (Figure 1b). Statistics such as vessel length distribution match anatomical observations but the placement of vessels relative to each other (called topology) is random.
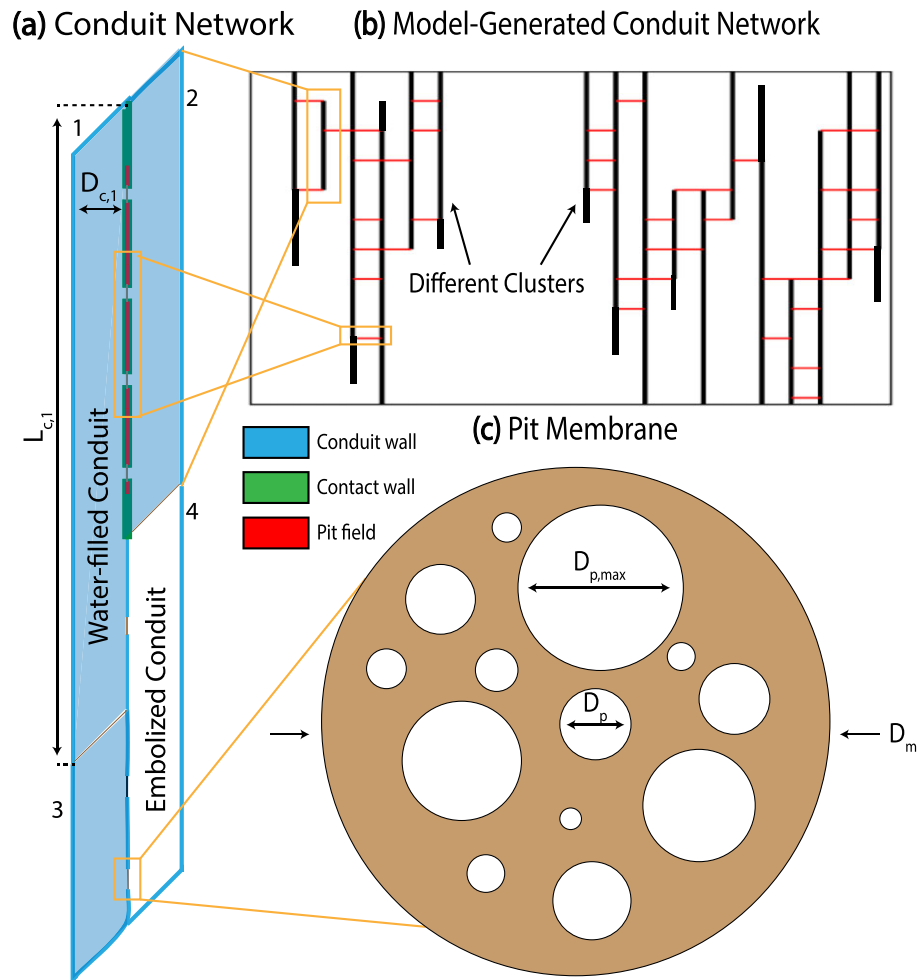
FIGURE 1 Model representation of pertinent xylem anatomical features and network structure. (a) Vessel network: Each of model's vessels corresponds to elements show on this conceptual drawing. Vessel 1 has a diameter $D_{v,1}$, a length $L_{v,1}$, a vessel wall (blue), a contact wall with another vessel (green), and a pit field (red). (b) Model-generated vessel network: Vertical black lines correspond to vessels. Horizontal red lines correspond to intervessel connections (IVCs). (c) Pit membrane: The structure of a pit membrane includes its membrane diameter (D_m), average pore diameter (D_p), and maximum pore diameter ($D_{p,max}$). Pit membrane pores are not drawn to scale. Other pit membrane structural properties, not shown here, include the membrane thickness T_m and the depth of the pit chamber that contains the membrane L_p [Colour figure can be viewed at wileyonlinelibrary.com]

2.2.1 | Vessels

The model starts by building vessels on the grid. Starting from the inlet node of the left-most column, the algorithm constructs a series of consecutive vessel elements by iterating through the nodes upward. At every node, there is a probability P_v, chosen a priori, that the model stops adding vessel elements and we designate that node as terminating. After a terminating node is reached, the model continues iterating through the nodes without constructing vessel elements. When an initiating node is reached again, with a probability NP_v also set a priori, the construction of a new series of consecutive vessel elements begins. The model continues building vessel elements following the same process until the final, outlet node in the current column is reached. At this point, the algorithm repeats in the adjacent column. All vessel elements have a set length L_{ve}. Vessels are defined as a continuous series of vessel elements and have as their extremities the initiating and terminating nodes of that series. Vessel length is specified as the number of vessel elements that it contains multiplied by L_{ve}. They

are constrained to the vertical direction and have constant diameter throughout their lengths. Choosing constant P_v and NP_v achieves an exponential distribution for vessel lengths (Figure S1; Nijsse, 2004). A higher P_v leads to longer vessels, on average, and a smaller NP_v reduces the vertical spacing between consecutive vessels.

As for vessel diameters, a lognormal probability density function describes their frequency of occurrences (Figure S2). The choice of a lognormal distribution is motivated by the need to ensure all diameters are positive valued and skewed and by actual vessel diameter frequency plots in flowering plant species (Cai & Tyree, 2010; Loepfe et al., 2007; Tyree & Zimmermann, 2002). The diameter of vessels is chosen such that the nth longest vessel adopts the nth largest sampled diameter that mimics the coordination between vessel length and diameter. The average of all vessel diameters in a given generated network is designated as D_v and the average of their lengths as L_v. D_v and L_v match the corresponding anatomical observations of the modelled species.

For tractability, the hydraulic contribution of every vessel is specified by the Hagen–Poiseuille relation for capillary tubes that determines the conductivity of an ideal cylindrical pipe of constant diameter under laminar (viscosity dominated) flow. It yields:

$$K_{v,i} = \frac{\pi D_{v,i}^4}{128 \mu L_{v,i}},$$ (1)

where $K_{v,i}$ is the hydraulic conductance of vessel i with diameter $D_{v,i}$ and length $L_{v,i}$ and μ is the water viscosity at 1 atm and 20°C. In reality, xylem vessels are far from ideal cylinders as they could contain wall thickenings, scalariform perforation plates, do not have a constant diameter throughout their lengths, and generally form a tortuous network that need not be vertically organized (Christman & Sperry, 2010; Jeje & Zimmermann, 1979; Tyree & Zimmermann, 2002).

2.2.2 | Intervessel connections and contact walls

Once vessels are formed, it is possible to build connections between them. The model starts by identifying vessels whose nodes are horizontally adjacent. These node pairs form a potential connection between those vessels. Out of all the potential connections in the network, the model randomly selects which ones will form IVCs, with a probability P_c. The choice of P_c affects how many IVCs exist in the network and how well vessels are connected to each other.

The surface area of an IVC is calculated as the average of the available wall surface area of the two vessels that it connects (Loepfe et al., 2007):

$$A_{IVC,k} = \frac{1}{2}\left(\frac{A_{v,i}}{N_{IVC,i}} + \frac{A_{v,j}}{N_{IVC,j}}\right)(f_c f_{pf}),$$ (2)

where $A_{IVC,k}$ is the area of pit field k that connects vessels i and j, A_v and N_{IVC} represent the surface area and number of IVCs on each vessel's wall, respectively. The f_c is the contact fraction between two vessels or the ratio of common wall area to total vessel surface area and f_{pf} is called the pit field fraction and is the ratio of that contact area occupied by pit membranes.

Tens to hundreds of pit membranes exist on a pit field area. Pit membranes are partially hydrolized primary cell walls and middle lamellas that allow the movement of water from vessel to vessel but limit the movement of gas and pathogens (Choat et al., 2006). The structure of vessel-to-vessel pits can be described using scanning electron microscopes and imaging techniques (Choat et al., 2006; Lens et al., 2011; Sperry & Hacke, 2004). Therefore, we can supply the model with measurements pertaining to pit membrane structure such as their average diameter (D_m), the average diameter of their aperture (D_a), their thickness (T_m), the diameter of the pores existing on them (D_p), and the depth of their chamber (L_p).

The number of pits $N_{m,k}$ that exist on IVC k, assuming equal membrane diameter ($=D_m$) for all pits, is calculated as follows:

$$N_{m,k} = \left\lfloor \frac{A_{IVC,k}}{\pi D_m^2/4} \right\rfloor.$$ (3)

Similarly for the number of pores $N_{p,k}$ on IVC k, an equation is developed and described elsewhere (Sperry & Hacke, 2004):

$$N_{p,k} = \left\lfloor \frac{A_{IVC,k}}{\pi (D_p + t_f)^2/4} \right\rfloor,$$ (4)

where t_f is the thickness of a microfibril strand taken to be 30 nm. We assume, for the sake of computing the number of pores, that all pores have equal diameter D_p. This will not be the case later on when cavitation resistance is discussed.

As a consequence, the hydraulic contribution of every IVC can now be specified. The hydraulic conductance associated with an IVC (K_{IVC}) is well approximated by a superposition of a Sampson flow resistance for pores in a plate of infinitesimal thickness and a Poiseuille flow contribution through the finite membrane thickness (Dagan, Weinbaum, & Pfeffer, 1982; Weissberg, 1962):

$$K_{IVC,k} = \frac{D_p^3 N_{p,k}}{24\mu}\left(1 + \frac{16 T_m}{3\pi D_p}\right)^{-1}.$$ (5)

The assumption made in Equations (3), (4), and (5) means that we are neglecting the influence of hydrodynamic interactions of closely spaced pores and the effect of varying pore sizes. Both of these neglected effects increase K_{IVC} (Jensen, Valente, & Stone, 2014), which means that the model might underestimate the hydraulic efficiency of IVCs. Moreover, the low asymptotic significance for the correlation between D_p and the xylem hydraulic conductivities reported elsewhere (Lens et al., 2011) suggests that K_{IVC} is in reality more strongly dependent on other structural and anatomical parameters such as the connectivity between vessels (Figure S3) and T_m than on D_p.

2.2.3 | Pit membrane cavitation resistance using the Young–Laplace equation

The air-seeding hypothesis is widely accepted as a mechanism for bubble or embolism propagation in xylem. For a vessel to become embolized by air-seeding, it is required that a bubble be present in one of its adjacent vessels (Tyree & Zimmermann, 2002). The presence of this bubble creates an interface between the bubble's contents (gas + air) and liquid water at every pore on the contact wall connecting them. Air-seeding additionally requires that the pressure difference between air and water at the interface exceed a threshold. That threshold could be set by surface tension as per the Young–Laplace equation. Once this threshold and the bubble adjacency requirement are met, the bubble is allowed to propagate instantly from one vessel to an adjacent one which further blocks part of the xylem network. Here, it is assumed that only the pore with largest diameter ($D_{p,\,max}$) in a contact wall is effective as it provides the easiest entry point for a bubble to a conductive vessel (Jarbeau, Ewers, & Davis, 1995). Therefore, we can write the equation for the bubble propagation pressure (BPP):

$$\Delta P = P_b - P_w \geq BPP = \frac{4\gamma}{D_{p,\,max}},$$ (6)

where P_w is the water pressure, P_b is the vapour-air bubble pressure, BPP is the P required for embolism to spread from one vessel to the adjacent one, and γ is the water surface tension at 1 atm and 20°C. As soon as Equation (6) is met, the newly embolized vessel further

impedes water transport in the network. Therefore, a binary view of vessel hydraulic health is adopted: It is either completely water filled or completely embolized. In the model, bubbles in a vessel cannot exist in a stable state, and all of them are assumed to grow large enough to fill the whole vessel instantaneously as soon as they penetrate it. There is evidence for this rapid expansion of air in embolized vessels based on calculations using air diffusion models and the Raleigh–Plesset equation (Hölttä, Vesala, & Nikinmaa, 2007; Konrad & Roth-Nebelsick, 2003).

The $D_{p, max}$ mentioned in the previous paragraph is not an easily measured quantity. In plants, the presence of hundreds to thousands of intervessel pit membranes each containing thousands of pores makes it challenging to find and measure the size of the largest one. There exist techniques other than direct measurement that help determine the largest pores and their presence (Venturas et al., 2016). In this paper, in order to predict VC location and curvature, $D_{p, max}$ is inferred statistically from the body of the probability density function describing measured pore diameters.

To proceed, we introduce further quantities related to contact walls. Because contact walls contain all the IVCs that connect the same vessels, we define N_{mc} and N_{pc} as the sum of all membranes ($\sum N_m$) and all pores ($\sum N_p$) of the constituting IVCs, respectively. Then, to assign a BPP to every contact wall in the generated network, the model does the following. First, the BPP of every pit membrane in the modelled network is prescribed from the same Weibull distribution. A Weibull distribution in terms of BPP is used because it is derived from Extreme Value Theory and describes heavy tails that allows the occurrence of rare and extremely low BPPs (and large corresponding pore diameters $D_{p, max}$; Equation (6)). The cumulative density function (CDF) of a pit membrane's BPP is $F_m(BPP)$ and it is given by the Weibull formula (Christman et al., 2009):

$$F_m(BPP) = 1 - \exp\left[-\left(\frac{BPP}{a}\right)^b\right], \tag{7}$$

where parameters a and b respectively represent a central value of BPPs (63rd percentile) and a measure of their variance. These parameters are to be determined using pore measurements (Methods S1). As explained above, it is the most extreme BPP or $D_{p, max}$ of the whole contact wall that matters for air-seeding. Therefore, we transform $F_m(BPP)$ to obtain the CDF of the BPP for each contact wall Christman et al., 2009):

$$F_{c,i}(BPP) = 1 - [1 - F_m(BPP)]^{N_{mc,i}} = 1 - \exp\left[-\left(\frac{BPP}{a/N_{mc,i}^{1/b}}\right)^b\right], \tag{8}$$

where $F_{c, i}(BPP)$ represents the CDF from which the BPP of contact wall i will be sampled. Equation (8) is a mathematical expression of the stochastic nature of pit membrane porosity based on contact wall area. In order to assess the effect of the stochasticity, the model can alternatively assign pit membrane porosities to contact walls, a priori, without knowledge of their area. This is called the deterministic regime of pit membrane porosity.

There are other theories pertaining to the permeability of angiosperm pit membranes to air bubbles. One such theory, not modelled here, stipulates that a large number of nanobubbles continuously form and collapse in xylem vessels. Nanobubbles are less than 200 nm in diameter and can cross the interface between air and water created by the noninterwoven layers of microfibrils of pit membranes. If the formed embryonic nanobubbles are mechanically stable (as may be predicted from the Young–Laplace equation) and their size does not grow, then they are harmless and not relevant to any VC inference. The stability of these nanobubbles depends on a number of features such as (a) whether they coalesce, (b) make contact with a solid surface (usually a destabilizing effect), and (c) the effect of the surfactants present on each bubble's surface (Jansen & Schenk, 2015; Schenk et al., 2017; Schenk, Steppe, & Jansen, 2015), among others. However, the precise mechanisms disturbing the stability of nanobubbles and their fate after destabilization are still under development and are beyond the scope here.

2.2.4 | Pit membrane cavitation resistance from the perspective of stretching

Studies have shown a significant statistical correlation between a plant organ's cavitation resistance and structural properties such as T_m, L_p, and D_a (Lens et al., 2011; Li et al., 2016). A pit membrane that connects a conductive vessel to an embolized one sustains a large pressure difference. This pressure difference could stretch the pit membranes enough for it to touch the walls of the chamber that contains it. Subsequent bulging of the membrane area within the pit aperture circumference leads to extensive pore stretching and potential permanent weakening of the pit's structural elements. That could lead to a decrease in a pit membrane's ability to stop embolism propagation (Sperry & Hacke, 2004; Tixier et al., 2014). This stretching, however, has only been observed occasionally as any pressure difference between either sides of the membrane is lost during sample preparations for electron microscopy.

Here, the model adopts the Kirchhoff–Love thin plate theory in the case of pure bending described elsewhere (Bauchau & Craig, 2009; Tixier et al., 2014). The pressure required for the membrane to touch the chamber walls P_b is the following:

$$\Delta P_b = \frac{1}{3} \frac{E}{1 - v^2} \frac{T_m^3}{\left(D_m^2 - D_a^2\right)^2} L_p, \tag{9}$$

where E is Young's modulus of elasticity of elasticity taken equal to 400 MPa (the value found for Populus deltoides; Capron, Tordjeman, Charru, Badel, & Cochard, 2014), v is the Poisson ratio taken equal to 0.3 based on the argument, presented elsewhere, that most polymers and cellulose were found to have similar values for this ratio (Tixier et al., 2014). D_a, the pit aperture diameter, is considered a constant fraction f_{ap} of D_m such that $D_a = f_{ap}D_m$. Finally, L_p, the pit chamber depth, is the distance from the centre of the pit membrane to the chamber wall.

The pressure at which stretched membranes allow bubble propagation is considered to be at a certain threshold strain that the membrane sustains. Therefore, a formulation for the maximum membrane strain, which is at the centre of the membrane, is adopted (Tixier et al., 2014):

$$\epsilon_{\max} = \frac{31 - v^2}{8} \frac{R^2}{E \; T_m^2} \Delta P, \tag{10}$$

where R is the radius of the stretched area. $R = \frac{D_m}{2}$ applies before the membrane touches the chamber wall, and $R = \frac{D_a}{2}$ applies after the P_b is achieved and the membrane rests on the chamber wall. In this framework, air-seeding is allowed to happen at a threshold amount of strain sampled from a normal distribution with mean e_{mean} and coefficient of variation e_{cv}. Following the stochastic argument that large contact walls are more vulnerable than small ones within the same tissue, the threshold strains that are sampled are distributed to each contact wall according to its area.

2.3 | Hydraulic properties and vulnerability curves

Once the xylem network is generated, we can start analyzing its hydraulics. The generated xylem network carries a flow of water under a prescribed pressure gradient applied between inlet and outlet (Figure 1b). This pressure gradient is not to be mistaken for the P applied for bubble propagation (Equation (6)). Flow through all nodes is calculated by imposing continuity everywhere except at the inlet and outlet. The total flow is then normalized by the prescribed pressure gradient and multiplied by the length of the network ($L_{ve} \times Rows$; Table 1) to obtain an intermediate conductivity value. This value is then normalized by the vessel cross-sectional area at two sections of the segment, equally spaced from either ends of the network, to obtain the maximum xylem area specific hydraulic conductivity $k_{xa, max}$.

To generate model VCs, we simulate the configuration used by the air pressurization technique (Cochard et al., 2013). The method relies on the demonstration that decreasing P_w under constant bubble pressure $P_b = 0.1 \; MPa$ or increasing P_b while keeping water pressure constant $P_w = 0.1 \; MPa$ leads to the same effect (Cochard, Cruiziat, & Tyree, 1992). Therefore, in what follows, when an increase in P is mentioned due to an increase in P_b, it is equivalent to a decrease in the suction pressure of water P_w that is equal in magnitude.

To assess a network's vulnerability to cavitation, a bubble is introduced in a random vessel in every cluster similar to the air-injection technique (Salleo et al., 1992; Sperry & Saliendra, 1994). By gradually pressurizing the air and gas inside the bubble, it is allowed to propagate when it satisfies the conditions set either by Equation (6) or Equation (10) (Figure 2). At each pressure increase, vessels may become embolized (light blue; Figure 2) causing other ones to become isolated and therefore unable to carry water anymore (pink; Figure 2). A collection of vessels and IVCs are isolated if they do not form a continuous path from inlet to outlet as a result of an embolism elsewhere in the network. At each P, we measure the hydraulic conductivity of the network as described above. We divide the obtained conductivity at that pressure by $k_{xa, max}$ (measured at $P = 0 \; MPa$) to obtain a percent loss of conductivity (PLC). Plotting PLC versus P yields the VC. The VC computed from the model is then fitted to a Weibull CDF, given as follows:

$$PLC(\Delta P) = 100 \left[1 - \frac{k_{xa} \Delta P}{k_{xa, \max}} \right] = 100 \left\{ 1 - \exp \left[- \left(\frac{\Delta P}{c} \right)^d \right] \right\}, \tag{11}$$

where the scaling parameter c determines the pressure at which PLC = 63%, a proxy for VC location along the pressure axis and parameter d represents the curvature of the VC. Note here the use of PLC = 63% instead of PLC = 50% for parameter c as this choice is compatible with Weibull CDF properties.

2.4 | Virtual experiments

The model was tested with direct anatomical observations (e.g., vessel and pit membrane sizes and distributions as well) made on fresh *A. glabrum* sections (Lens et al., 2011; Table 1). Our choice was motivated by a complete characterization of xylem anatomical features and in particular for the high number of pore size measurements per contact wall area for this species compared with measurements made on other species. We consider the two cavitation resistance schemes of pit membranes separately in the sections that follow.
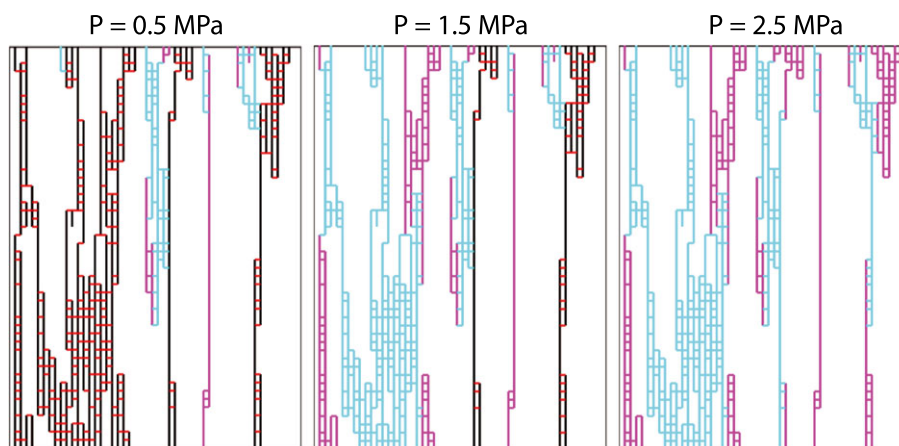
P = 0.5 MPa   P = 1.5 MPa   P = 2.5 MPa

FIGURE 2 Embolism spread in a model-generated xylem network as the pressure difference between air and water increases. Black vertical lines represent water-filled vessels and red horizontal lines represent intervessel connections (IVCs). For easier visualization of the pit membranes, horizontal grid lines are not to scale. Left: One initial embolism randomly located in each cluster, light blue: embolized vessels and IVCs, pink: isolated vessels and IVCs. As the pressure difference is increased incrementally (left to right), initial embolisms propagate. Simulation continues until both clusters become completely disconnected and nonconducting [Colour figure can be viewed at wileyonlinelibrary.com]

3 | RESULTS

To evaluate the ability of the model to upscale plant hydraulics from the microscopic, anatomical processes to the whole plant tissue, we generate three xylem networks with parameters set to match anatomical measurements of *A. glabrum*. The model relies solely on these measurements and none that represent whole tissue characteristics such as empirical VCs or measurements of maximum hydraulic conductance. Here, the Young–Laplace equation based on the maximum pore diameter is used as a prognostic case. The three model-generated networks differ only in the Weibull sampling distributions of pit membrane porosity (i.e., scaling parameter a of Equation (8); Methods S1). The right-most of the computed VCs from these model-generated networks closely matches the empirical VC of that same species in terms of location along the P axis and curvature (Figure 3a). The empirical VC was measured using the standard centrifuge method (Lens et al., 2011). The value of the scaling parameter a used for the matching VC is 20.28 MPa and the value of parameter b is 3.2 (Equation (8)).

Vessel water relations can also be computed with this model (Figure 4; Methods S2). By vessel water, we imply the water that is still available in vessels that are conductive or isolated but not embolized. We use the term vessel water to distinguish it from total water because vessel water does not include the water in living parenchyma cells (Domec & Gartner, 2001; Hölttä, Cochard, Nikinmaa, & Mencuccini, 2009; Huang et al., 2017). The model calculations suggest some 40–60% of the initial vessel water is still present but mostly isolated, even when *PLC* > 90% (Figure 4). This value is in agreement with expectations from many studies where around half of the total water is trapped in the plant at hydraulic failure (Domec & Gartner, 2003; Loepfe et al., 2007; Pratt & Jacobsen, 2017; Pratt & Jacobsen, 2018).

An alternate account of cavitation resistance based on pit membrane stretching can be used to upscale plant water relations (Figure 3b). The parameters of this framework, e_{mean} and e_{cv}, were tuned to achieve a match between model and empirical VCs. Therefore, we treat this method of cavitation resistance as a diagnostic case that serves to showcase the versatility of the model and its ability to support different parameterizations of microscopic processes. The most satisfactory result was achieved for e_{mean} = 0.015 and e_{cv} = 0.35, and aspiration was necessary for air-seeding to occur.

Additionally, results suggest that initial embolism location in every cluster alters VC location along the ΔP axis and its slope. We therefore ensemble-average multiple simulations to cancel the effect of initial embolism location on VCs. Table 2 shows correlations and corresponding asymptotic significance between model inputs and outputs. Judging by the asymptotic significance (P values; not to be confused with pressure), average vessel diameter D_v and length L_v affect k_{xa}, P_{10}, and the scaling parameter c or P_{63} as expected. Although L_v alters P_{90}, D_v does not. The dependence of VC location (i.e., P_{10}, P_{63}, and P_{90}) on average pit membrane diameter D_m is a consequence of the stochastic nature of pit membrane porosity. Larger D_m leads to a smaller number of pit membranes which leads to higher bubble propagation pressure *BPP* and less vulnerable vessels (Equations (3) and (8)). Therefore, VC location also
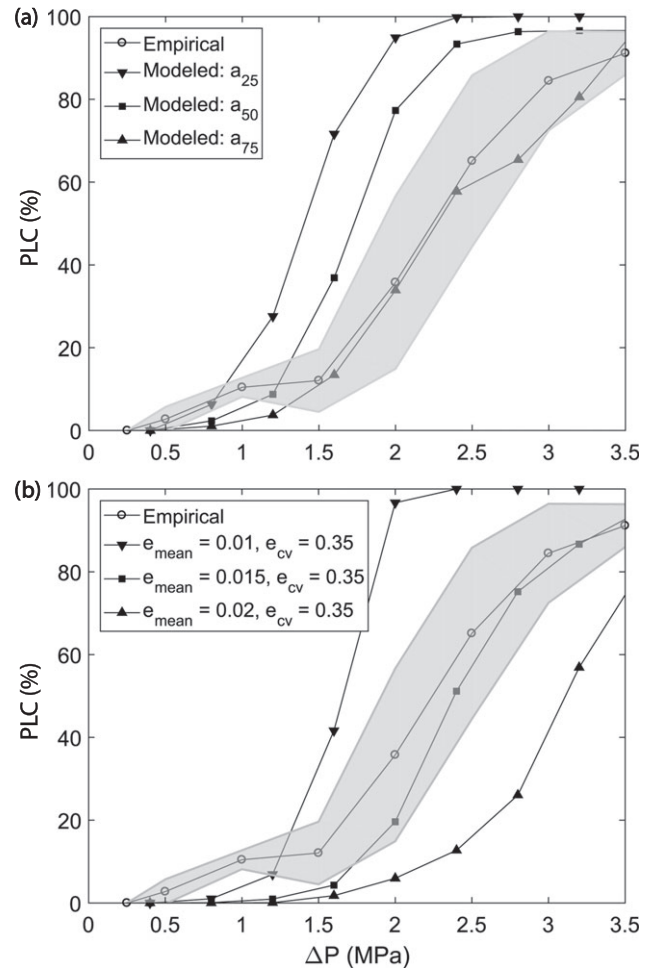

FIGURE 3 (a) *Acer glabrum* empirical vulnerability to embolism curve (VC; Lens et al., 2011) along with three model-generated VCs using the Young–Laplace formulation of cavitation resistance. Model parameters used to generate the xylem network VCs correspond to those in Table 1. Parameter a of Equation (7) is the 63rd percentile of pit membrane bubble propagation pressure. There are three candidate values for parameter a: a_{25}, a_{50}, and a_{75}. These candidate values are derived from real observations of pore measurements (Method S1). Shaded area covers the mean and standard deviation of the empirical VC. (b) Diagnostic prediction of VC shape using the pit membrane stretching perspective of cavitation resistance. The values of mean strain at hydraulic failure e_{mean} and its coefficient of variation e_{cv} were tuned to reach satisfactory VCs

depends on contact fraction f_c and pit field fraction f_{pf} which also factor into the determination of the number of pit membranes per contact wall N_{mc} through Equations (2) and (3). The model's mean conductivity value k_{xa} for *Acer glabrum* is 5.3 $g. \, s^{-1} \cdot m^{-1} \cdot kPa^{-1}$ (Table S1).

The linkage between vessel-scale and pit-scale dimensions also affects the upscaling of hydraulics from the microscopic to the macroscopic. Keeping all vessel and pit dimensions constant while varying how the porosity of the pit membranes is prescribed for every vessel has a considerable effect on VCs (Figure 5). Compared with the stochastic regime, the deterministic regime exhibits steeper VCs. This is due to an increase in the lower arm of the VCs, namely, P_{10} and P_{50} to a lesser degree, whereas the upper arm remains intact. The fraction of vessels embolized at P_{90} does not vary significantly under the two regimes (Figure S5).
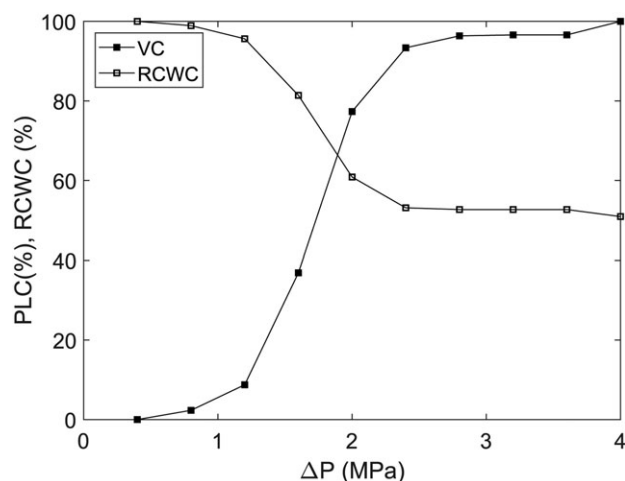
FIGURE 4 Vulnerability to embolism curve (VC) and relative conduit water content (RCWC) variation with an increase in P of a single model run. RCWC is the fraction of the initial volume of water still existing inside vessels. Model parameters correspond to those in Table 1 following measurement of *Acer glabrum* stems

The mechanism giving rise to this change in VC shape on the microscopic scales is an increased resistance to cavitation of long and wide vessels under the deterministic regime of pit membrane porosity prescription (Figure 6). However, at 3.5 MPa, well beyond PLC = 90% for most of the simulations in both sets, the bar graphs are almost identical. This indicates that hydraulic failure still occurs at the same P under the deterministic and stochastic porosity regimes even though the onset of loss of conductivity happens at a higher P in the former case.

4 | DISCUSSION

4.1 | Model upscaling of microscopic hydraulics

The two-dimensional nature of the xylem networks generated by this model is a plausible representation of several *Acer* species, namely, *A. glabrum*, as these species exhibit a mix between solitary vessels and vessels arranged in radial multiples (Figure 7). Hence, for the pur-

TABLE 2 r values between model network input statistics (columns) and computed outputs

	D_v	L_v	$D_{v,cv}$	D_m	D_p	f_v	f_{pf}	T_m
Parameter c	−0.31**	−0.19*	−0.20*	0.85**	<0.01	−0.85**	−0.5**	0.12
Parameter d	−0.11	−0.02	−0.07	<0.01	−0.03	<0.01	0.06	0.15
P_{10}	−0.32**	−0.21*	−0.29**	0.73**	−0.06	−0.83**	−0.42**	0.24*
P_{90}	−0.16	−0.22**	−0.16	0.81**	−0.04	−0.79**	−0.49**	0.02
%embolized	0.15	0.58**	−0.04	−0.07	−0.04	−0.21*	0.14	0.26**
$k_{xa,max}$	0.73**	0.64**	0.27**	0.09	0.75**	0.46**	0.33**	−0.11

Note. The varied parameters are the average vessel diameter (D_v), the average vessel length (L_v), the coefficient of variation in vessel diameter ($D_{v,cv}$), the pit membrane diameter (D_m), the pore diameter (D_p), the contact fraction (f_c), the pit field fraction (f_{pf}), the pit aperture area fraction (f_{ap}), the pit membrane thickness (T_m), and the pit chamber depth (L_p). The output variables that represent whole-segment hydraulics are the scaling parameter of the Weibull fit to the vulnerability curve (c), curvature parameter (d) of that fit, the pressure at which 10% of the segment conductivity is lost (P_{10}), pressure at 90% loss of conductivity (P_{90}), the fraction of embolized vessels at P_{90} (%embolized), and the maximum xylem area specific hydraulic conductivity of the segment ($k_{xa,max}$).
*P < 0.1; **P < 0.01.

FIGURE 5 Boxplots showing the effect of using a stochastic versus a deterministic approach to pit membrane cavitation resistance. In the stochastic approach, large contact wall areas are more likely to hold larger pores than their smaller counterparts in the same segment. The effect is shown on the pressures at which 10% (P_{10}) and 90% loss of conductivity occurred (P_{90}), as well as the Weibull scaling parameter (c = P_{63}) and curvature parameter d of Equation (11). A higher value for parameter d means that the VC is steeper. The middle horizontal line in the box represents the median, the lower and upper horizontal box borders represent 25th and 75th percentiles, respectively, and the extrema of the whiskers encompass the rest of the data not considered outliers. Outliers are plotted using the "+" symbol
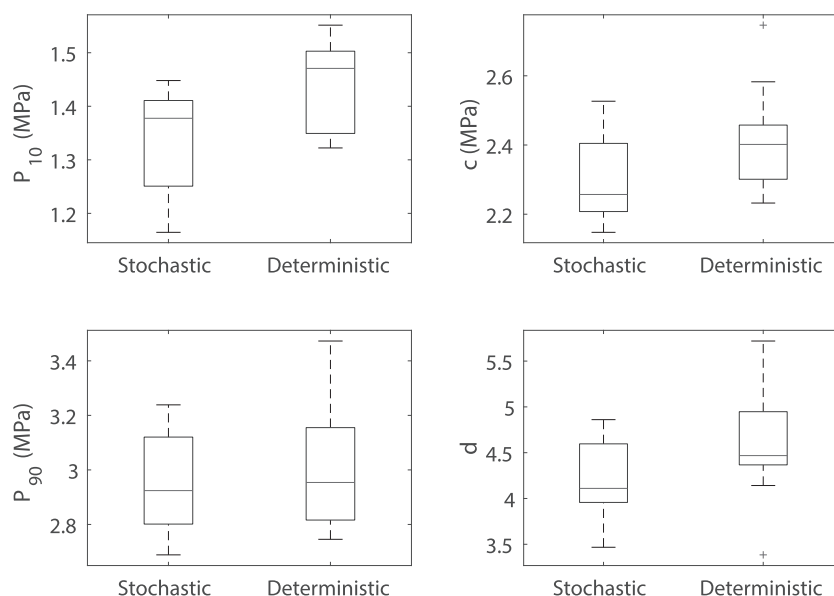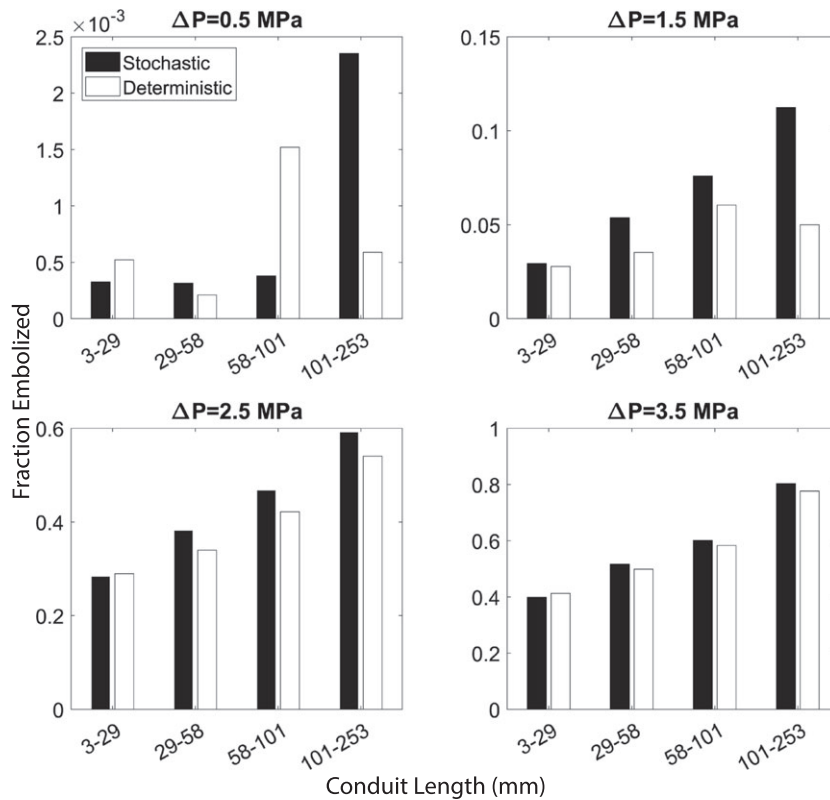
FIGURE 6 Frequency of embolized vessels at different xylem pressure *P*, showing that long vessels are less vulnerable to cavitation at low *P* when the deterministic regime of pit membrane porosity is used compared with the stochastic regime
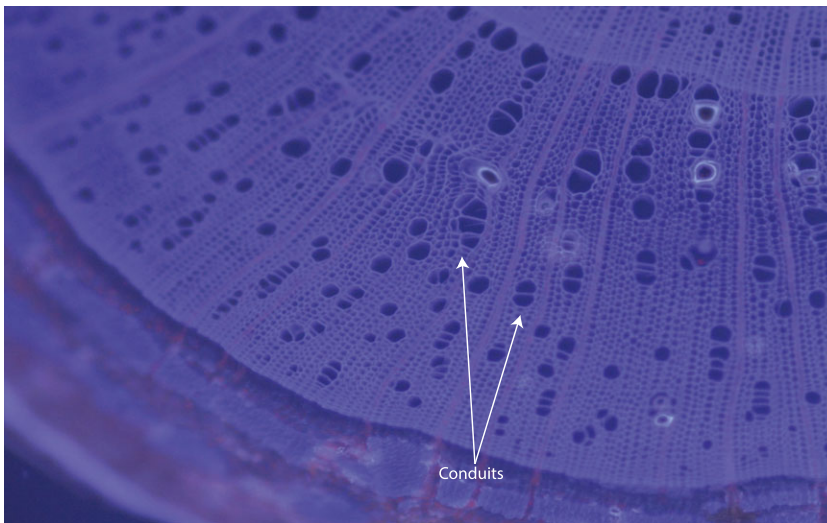

FIGURE 7 *Acer glabrum* stem cross section showing vessels in solitary and radial arrangements. The model's two-dimensional nature is therefore a plausible representation of this species [Colour figure can be viewed at wileyonlinelibrary.com]

poses of modelling VCs from water and bubble transport, the relevant dimensions are mainly the radial and axial ones adhering to a two-dimensional flow pattern.

It was shown elsewhere that different species of the genus *Acer* sample their pore sizes from different distributions $F_m(BPP)$ at the pit membrane level (Equation (7); Christman et al., 2009). This means that species with larger mean pit area could still be less vulnerable to embolism spread than one with smaller mean pit area if it samples pores from a more conservative $F_m(BPP)$. In this study, the rare pit hypothesis (Christman et al., 2009; Wheeler et al., 2005) was bypassed by resorting to a stochastic prescription of pit membrane porosity. Under this scheme, because we assume that the contact f_c and pit

field fractions f_{pf} are the same throughout the same plant organ, large vessels with larger wall area are more vulnerable to cavitation than small ones in the same tissue. However, other tissues with smaller average vessel diameter D_v should not have to be more resistant to cavitation, as the rare pit hypothesis predicts, if other anatomical properties are different.

The model derives $F_m(BPP)$ solely from anatomical measurements and scaling arguments. The scaling arguments are required because the largest pore in a contact wall occurs approximately once in a thousand pores and measuring them all is a labour-intensive task. Furthermore, pit membranes stretch during water flow through plant tissues making them more vulnerable. In fact, it has been shown that pit

membrane thickness (T_m) is strongly correlated to cavitation resistance (Lens et al., 2011; Li et al., 2016). However, the magnitude of stretching and the stretched size of the pores are unknown, and their measurement has not been attempted. Despite these challenges, the scaling arguments used in this study yield a good fit to empirical VCs for an *Acer* species (Figure 3a). As such, the computed VC using the Young–Laplace equation for pit membrane cavitation resistance provides a prognostic exhibit of the model's ability to correctly upscale microscopic hydraulics.

To show the model's versatility, a different scheme of pit membrane cavitation resistance based on its stretching is used. Because the required measurements were not available, a diagnostic perspective is adopted. That is, the mean membrane strain at cavitation e_{mean}, and its coefficient of variation e_{cv} have been tuned to yield a match in computed and empirical VCs where the optimized parameters were then shown to be plausible. This diagnostic point of view highlights the use of the proposed model to explore multiple hypotheses about resistance to cavitation. The benefit here is pinpointing "equi-finality" issues where multiple resistance to cavitation mechanisms still yield similar outcomes when tested against VC shapes.

The scaling arguments used to determine the bubble propagation pressure (BPP) in the Young–Laplace equation are not expected to hold for every species. Deriving the stretched dimensions of extreme pores is experimentally challenging. What matters most in the context of whole-segment loss of conductivity is how frequent the extremes occur. Information on this frequency is embedded in the tail of the distribution of pore diameters (proportional to the inverse of *BPP* and, therefore, $F_m(BPP)$). Pores can enlarge when the pit membranes are stretched (Sperry & Hacke, 2004; Tixier et al., 2014), and the degree of stretching of a pit membrane is related to its thickness T_m among other structural properties. So a plausible hypothesis for a future work would be that T_m provides information on the "fatness" of the tail of the distribution of pit membrane pore diameters. However, measuring such structural properties of a thin, fragile pit membrane is challenging because much of it is altered in the process of preparing a sample for observation under a microscope.

4.2 | The linkage between vessel-scale and pit-scale properties affects the vulnerability curve

The linkage between the two microscopic scales (vessel-scale and pit-scale) is embedded in how pit membrane porosity is prescribed. Two plant tissues having the same anatomical statistics could exhibit differing cavitation resistance behaviours if this linkage is different. The two ingredients forming this linkage are vessel connectivity (Figure S3) and the dependence of pit membrane porosity on the area of a contact wall (Figure S4). Within the same plant tissue, when a vessel is connected to five others, for instance, it is more likely to be adjacent to an embolism than another vessel connected to two other vessels. The highly connected vessel has also more entry points for bubbles to propagate and inhibit its hydraulic capabilities. Furthermore, the effect of higher connectivity is exacerbated when pit membrane porosity is dependent on contact wall area. Because, in the

model, highly connected vessels are usually the longest and widest within a particular plant tissue, they are more likely to have larger pores due to their large A_p. So there is a dual risk in being a large vessel. It is stressed that this discussion only applies when vessels within the same plant tissue are compared with one another and not to vessels in other plant tissues especially ones from different species. However, in some *Acer* species, the long vessels tend to be more solitary than shorter ones.

To show the effect of the dependence of pit membrane porosity on A_p within the same segment (the stochastic case), the model can also artificially prescribe contact wall cavitation resistance a priori, neglecting its area (the deterministic case), and observe differences in whole-segment hydraulics. There is a significant difference in the shape of VCs under the two cases (Figure 5). Under the deterministic case, large vessels that are behind most of the conductive ability of a plant tissue are shielded from embolism by more resistant contact walls (Figure 6). This delays the onset of significant segment loss of conductivity (P_{10}) but does not alter the pressure at which hydraulic failure could occur (P_{90}) which results in a steeper VC.

This result could have implications beyond those shown in the current study: If the linkage between the two microscopic scales could alter VC shape significantly, then this points to the necessity of better understanding three-dimensional xylem network topology to decipher mechanisms between different observed VC shapes.

The accuracy of the stochastic mechanism determining pit membrane porosity in this model depends on how pit membrane structural properties vary with vessels of different sizes in real plants. A recent study showed that larger vessels have thicker pit membranes that are thought to be less permeable to embolism propagation (Pfautsch et al., 2018). Variations like that suggests that using a single pore size sampling distribution at the pit membrane level ($F_m(BPP)$; Equation (7)) is restrictive. Furthermore, additional research on the three-dimensional network structure of xylem is required to confirm relations such as the correlation between contact wall area and vessel lumen area.

To summarize, a model of flowering plant xylem is proposed to discern how wood anatomy and plant hydraulic function are linked. Because the detailed mechanism of embolism spread through angiosperm pit membrane is under debate, we use different porosity schemes: one based on the largest pore and the other on membrane stretching. This model is capable of upscaling hydraulics from the pit-level all the way up to the whole-segment level. Additionally, it was shown that the way the vessel- and pit-scale dimensions are linked can alter VC shape even when anatomical statistics remain unaltered. This underscores the importance of stepping up research related to xylem network topology to understand its effect on plant hydraulics and resistance to drought. Future research that yields improved mathematical and physical bases to the process of cavitation in angiosperms can easily be incorporated into the model to improve its results. In the future, this model is expected to serve as a research tool to generate and test hypotheses about the role of xylem characteristics that are not easily observed or measured, such as the connectivity between vessels, as these have been shown to affect VC shape strikingly.

ORCID

Assaad Mrad http://orcid.org/0000-0003-4922-4446
Jean-Christophe Domec http://orcid.org/0000-0003-0478-2559
Frederic Lens http://orcid.org/0000-0002-5001-0149
Gabriel Katul http://orcid.org/0000-0001-9768-3693

REFERENCES

Adams, H. D., Zeppel, M. J. B., Anderegg, W. R. L., Hartmann, H., Landhäusser, S. M., Tissue, D. T., ... McDowell, N. G. (2017). A multi-species synthesis of physiological mechanisms in drought induced tree mortality. *Nature Ecology and Evolution*, 1(9), 1285–1291.

Anderegg, W. R. L., Klein, T., Bartlett, M., Sack, L., Pellegrini, A. F. A., Choat, B., & Jansen, S. (2016). Meta-analysis reveals that hydraulic traits explain cross-species patterns of drought induced tree mortality across the globe. *Proceedings of the National Academy of Sciences*, 113(18), 5024–5029. arXiv: arXiv:1408.1149

Bauchau, O., & Craig, J. (2009). Kirchhoff plate theory. *Structural analysis*. Springer, pp. 819–914.

Brodersen, C. R., & Roddy, A. B. (2016). New frontiers in the three-dimensional visualization of plant structure and function. *American Journal of Botany*, 103(2), 184–188.

Cai, J., Li, S., Zhang, H., Zhang, S., & Tyree, M. T. (2014). Recalcitrant vulnerability curves: Methods of analysis and the concept of fibre bridges for enhanced cavitation resistance. *Plant, Cell and Environment*, 37(1), 35–44.

Cai, J., & Tyree, M. T. (2010). The impact of vessel size on vulnerability curves: Data and models for within-species variability in saplings of aspen, Populus tremuloides Michx. *Plant, Cell & Environment*, 33(7), 1059–1069.

Capron, M., Tordjeman, P., Charru, F., Badel, E., & Cochard, H. (2014). Gas flow in plant microfluidic networks controlled by capillary valves. *Physical Review E - Statistical, Nonlinear, and Soft Matter Physics*, 89, 3.

Choat, B., Brodie, T. W., Cobb, A. R., Zwieniecki, M. A., & Holbrook, N. M. (2006). Direct measurements of intervessel pit membrane hydraulic resistance in two angiosperm tree species. *American Journal of Botany*, 93(7), 993–1000.

Choat, B., Cobb, A. R., & Jansen, S. (2008). Structure and function of bordered pits: New discoveries and impacts on whole-plant hydraulic function. *New Phytologist*, 177(3), 608–626.

Choat, B., Jansen, S., Brodribb, T. J., Cochard, H., Delzon, S., Bhaskar, R., ... Zanne, A. E. (2012). Global convergence in the vulnerability of forests to drought. *Nature*, 491(7426), 752–755.

Christman, M., & Sperry, J. (2010). Single-vessel flow measurements indicate scalariform perforation plates confer higher flow resistance than previously estimated. *Plant, Cell & Environment*, 33(3), 431–443.

Christman, M., Sperry, J., & Adler, F. (2009). Testing the 'rare pit' hypothesis for xylem cavitation resistance in three species of Acer. *New Phytologist*, 182(3), 664–674.

Cochard, H., Badel, E., Herbette, S., Delzon, S., Choat, B., & Jansen, S. (2013). Methods for measuring plant vulnerability to cavitation: A critical review. *Journal of Experimental Botany*, 64(15), 4779–4791.

Cochard, H., Cruiziat, P., & Tyree, M. (1992). Use of positive pressures to establish vulnerability curves: Further support for the air-seeding hypothesis and implications for pressure-volume analysis. *Plant Physiology*, 100(1), 205–209.

Dagan, Z., Weinbaum, S., & Pfeffer, R. (1982). An infinite-series solution for the creeping motion through an orifice of finite length. *Journal of Fluid Mechanics*, 115, 505–523.

Domec, J. C., & Gartner, B. (2003). Relationship between growth rates and xylem hydraulic characteristics in young, mature and old-growth ponderosa pine trees. *Plant, Cell & Environment*, 26, 471–483.

Domec, J. C., & Gartner, B. L. (2001). Cavitation and water storage capacity in bole xylem segments of mature and young Douglas-fir trees. *Trees*, 15(4), 204–214.

Haberlandt, G., & Drummond, M. (1914). *Physiological plant anatomy*. London, UK: Macmillan and Company, limited.

Hacke, U., Sperry, J., Wheeler, J., & Castro, L. (2006). Scaling of angiosperm xylem structure with safety and efficiency. *Tree Physiology*, 26(6), 689–701.

Hölttä, T., Cochard, H., Nikinmaa, E., & Mencuccini, M. (2009). Capacitive effect of cavitation in xylem conduits: Results from a dynamic model. *Plant, Cell & Environment*, 32(1), 10–21.

Hölttä, T., Vesala, T., & Nikinmaa, E. (2007). A model of bubble growth leading to xylem conduit embolism. *Journal of Theoretical Biology*, 249(1), 111–123.

Huang, C. W., Domec, J. C., Ward, E. J., Duman, T., Manoli, G., Parolari, A. J., & Katul, G. G. (2017). The effect of plant water storage on water fluxes within the coupled soil-plant system. *New Phytologist*, 213(3), 1093–1106.

Hunt, A. G., & Manzoni, S. (2015). Water transport in plants. *Networks on Networks*. 20532571. Morgan & Claypool Publishers, pp. 1–13.

Jacobsen, A. L., Pratt, R. B., Tobin, M. F., Hacke, U. G., & Ewers, F. W. (2012). A global analysis of xylem vessel length in woody plants. *American Journal of Botany*, 99(10), 1583–1591.

Jansen, S., & Schenk, H. J. (2015). On the ascent of sap in the presence of bubbles. *American Journal of Botany*, 102(10), 1561–1563.

Jarbeau, J. A., Ewers, F. W., & Davis, S. D. (1995). The mechanism of water-stress-induced embolism in two species of chaparral shrubs. *Plant, Cell & Environment*, 18(2), 189–196.

Jeje, A. Y. A., & Zimmermann, M. H. (1979). Resistance to water flow in xylem vessels. *Journal of Experimental Botany*, 30(4), 817–827.

Jensen, K., Valente, A., & Stone, H. (2014). Flow rate through microfilters: Influence of the pore size distribution, hydrodynamic interactions, wall slip, and inertia. *Physics of Fluids*, 26(5), 52004.

Johnson, D. M., et al. (2018). Co-occurring woody species have diverse hydraulic strategies and mortality rates during an extreme drought. *Plant, Cell & Environment*, 41(3), 576–588.

Katul, G., Porporato, A., & Oren, R. (2007). Stochastic dynamics of plant-water interactions. *Annual Review of Ecology, Evolution, and Systematics*, 38(1), 767–791.

Knipfer, T., Brodersen, C. R., Zedan, A., Kluepfel, D. A., & McElrone, A. J. (2015). Patterns of drought-induced embolism formation and spread in living walnut saplings visualized using X-ray microtomography. *Tree Physiology*, 35(7), 744–755.

Konrad, W., & Roth-Nebelsick, A. (2003). The dynamics of gas bubbles in conduits of vascular plants and implications for embolism repair. *Journal of Theoretical Biology*, 224(1), 43–61.

Larter, M., Brodribb, T. J., Pfautsch, S., Burlett, R., Cochard, H., & Delzon, S. (2015). Extreme aridity pushes trees to their physical limits. *Plant Physiology*, 168(3), 804–807.

Lens, F., Sperry, J., Christman, M., Choat, B., Rabaey, D., & Jansen, S. (2011). Testing hypotheses that link wood anatomy to cavitation resistance and hydraulic conductivity in the genus Acer. *New Phytologist*, 190(3), 709–723.

Li, S., Lens, F., Espino, S., Karimi, Z., Klepsch, M., Schenk, H. J., ... Jansen, S. (2016). Intervessel pit membrane thickness as a key determinant of embolism resistance in angiosperm xylem. *IAWA Journal*, 37(2), 152–171.

Loepfe, L., Martinez-Vilalta, J., Piñol, J., & Mencuccini, M. (2007). The relevance of xylem network structure for plant hydraulic efficiency and safety. *Journal of Theoretical Biology*, 247(4), 788–803.

Lucas, W. J., Groover, A., Lichtenberger, R., Furuta, K., Yadav, S. R., Helariutta, Y., … Kachroo, P. (2013). The plant vascular system: Evolution, development and functions. *Journal of Integrative Plant Biology*, 55(4), 294–388.

Manzoni, S., Katul, G., & Porporato, A. (2014). A dynamical system perspective on plant hydraulic failure. *Water Resources Research*, 50(6), 5170–5183.

McElrone, A. J., Choat, B., Parkinson, D. Y., MacDowell, A. A., & Brodersen, C. R. (2013). Using high resolution computed tomography to visualize the three dimensional structure and function of plant vasculature. *Journal of Visualized Experiments: JoVE*, 74. https://doi.org/10.1111/pce.12680

Meinzer, F. C., Clearwater, M. J., & Goldstein, G. (2001). Water transport in trees: Current perspectives, new insights and some controversies. *Environmental and Experimental Botany*, 45(3), 239–262.

Nijsse, J. (2004). On the mechanism of xylem vessel length regulation. *Plant Physiology*, 134(1), 32–34.

Pfautsch, S., Aspinwall, M. J., Drake, J. E., Chacon-Doria, L., Langelaan, R. J., Tissue, D. T., … Lens, F. (2018). Traits and trade-offs in whole-tree hydraulic architecture along the vertical axis of Eucalyptus grandis. *Annals of Botany*, 121(1), 129–141.

Pratt, R. B., & Jacobsen, A. L. (2017). Conflicting demands on angiosperm xylem: Tradeoffs among storage, transport and biomechanics. *Plant, Cell & Environment*, 40(6), 897–913.

Pratt, R. B., & Jacobsen, A. L. (2018). Identifying which conduits are moving water in woody plants: A new HRCT-based method. *Tree Physiology*..

Salleo, S., Hinckley, T., Kikuta, S., Gullo, M., Weilgony, P., Yoon, T. M., & Richter, H. (1992). A method for inducing xylem emboli in situ: Experiments with a field-grown tree. *Plant, Cell & Environment*, 15(4), 491–497.

Schenk, H. J., Espino, S., Romo, D. M., Nima, N., Do, A. Y. T., Michaud, J. M., … Jansen, S. (2017). Xylem surfactants introduce a new element to the cohesion-tension theory. *Plant Physiology*, 173(2), 1177–1196.

Schenk, H. J., Steppe, K., & Jansen, S. (2015). Nanobubbles: A new paradigm for air-seeding in xylem. *Trends in Plant Science*, 20(4), 199–205.

Scholz, A., Rabaey, D., Stein, A., Cochard, H., Smets, E., & Jansen, S. (2013). The evolution and function of vessel and pit characters with respect to cavitation resistance across 10 Prunus species. *Tree Physiology*, 33(7), 684–694.

Sperry, J. (2011). Hydraulics of vascular water transport. In P. Wojtaszek (Ed.), *Mechanical integration of plant cells and plants* (pp. 303–327). Berlin, Heidelberg: Springer Berlin Heidelberg.

Sperry, J., & Hacke, U. (2004). Analysis of circular bordered pit function I. Angiosperm vessels with homogenous pit membranes. *American Journal of Botany*, 91(3), 369–385.

Sperry, J., & Saliendra, N. (1994). Intra-and inter-plant variation in xylem cavitation in *Betula occidentalis*. *Plant, Cell & Environment*, 17(11), 1233–1241.

Sperry, J. S. (2003). Evolution of water transport and xylem structure. *International Journal of Plant Sciences*, 164(S3), S115–S127.

Tixier, A., Herbette, S., Jansen, S., Capron, M., Tordjeman, P., Cochard, H., & Badel, E. (2014). Modelling the mechanical behaviour of pit membranes in bordered pits with respect to cavitation resistance in angiosperms. *Annals of Botany*, 114(2), 325–334.

Tyree, M. T., & Zimmermann, M. H. (2002). *Xylem structure and the ascent of sap* (2nd ed.)*Springer Series in Wood Science*. (p. 284). Berlin, Heidelberg: Springer Berlin Heidelberg.

Venturas, M. D., Rodriguez-Zaccaro, F. D., Percolla, M. I., Crous, C. J., Jacobsen, A. L., & Pratt, R. B. (2016). Single vessel air injection estimates of xylem resistance to cavitation are affected by vessel network characteristics and sample length. *Tree Physiology*, 36(10), 1247–1259.

Weissberg, H. L. (1962). End correction for slow viscous flow through long tubes. *Physics of Fluids*, 5(9), 1033.

Wheeler, J., Sperry, J., Hacke, U., & Hoang, N. (2005). Inter-vessel pitting and cavitation in woody Rosaceae and other vessel led plants: A basis for a safety versus efficiency trade-off in xylem transport. *Plant, Cell & Environment*, 28(6), 800–812.

SUPPORTING INFORMATION

Additional supporting information may be found online in the Supporting Information section at the end of the article.